

An explanation for the difference between twentieth and twenty-first century land–sea warming ratio in climate models

M. M. Joshi · F. H. Lambert · M. J. Webb

Received: 26 June 2012 / Accepted: 2 January 2013 / Published online: 16 January 2013
© Springer-Verlag Berlin Heidelberg 2013

Abstract A land–sea surface warming ratio (or φ) that exceeds unity is a robust feature of both observed and modelled climate change. Interestingly, though climate models have differing values for φ , it remains almost time-invariant for a wide range of twenty-first century climate transient warming scenarios, while varying in simulations of the twentieth century. Here, we present an explanation for time-invariant land–sea warming ratio that applies if three conditions on radiative forcing are met: first, spatial variations in the climate forcing must be sufficiently small that the lower free troposphere warms evenly over land and ocean; second, the temperature response must not be large enough to change the global circulation to zeroth order; third, the temperature response must not be large enough to modify the boundary layer amplification mechanisms that contribute to making φ exceed unity. Projected temperature changes over this century are too small to breach the latter two conditions. Hence, the mechanism appears to show why both twenty-

first century and time-invariant CO₂ forcing lead to similar values of φ in climate models despite the presence of transient ocean heat uptake, whereas twentieth century forcing—which has a significant spatially confined anthropogenic tropospheric aerosol component that breaches the first condition—leads to modelled values of φ that vary widely amongst models and in time. Our results suggest an explanation for the behaviour of φ when climate is forced by other regionally confined forcing scenarios such as geo-engineered changes to oceanic clouds. Our results show how land–sea contrasts in surface and boundary layer characteristics act in tandem to produce the land–sea surface warming contrast.

Keywords Climate change · Climate modelling · Surface temperature · Radiative forcing

1 Introduction

The land–sea warming contrast is a well-known phenomenon whereby large parts of the land surface undergo greater warming in response to climate forcing than the ocean (Manabe et al. 1991). It is robust amongst climate models and also displayed in observations of the late twentieth century (Sutton et al. 2007). Somewhat counter-intuitively, a land–sea surface warming ratio (henceforth φ) greater than unity during transient climate change is actually not mainly a result of the differing thermal inertias of land and ocean, but primarily originates in the differing properties of the surface and boundary layer (henceforth BL) over land and ocean (Manabe et al. 1991; Sutton et al. 2007; Joshi et al. 2008 (henceforth JGW08), Dong et al. 2009) as well as differing cloud feedbacks (Fasullo 2010; Andrews et al. 2010).

M. M. Joshi
NCAS Climate, Department of Meteorology, University
of Reading, Earley Gate, PO Box 243, Reading RG6 6BB, UK

Present Address:
M. M. Joshi (✉)
Department of Environmental Sciences, University of East
Anglia, Norwich Research Park, Norwich NR4 7TJ, UK
e-mail: m.joshi@uea.ac.uk

F. H. Lambert
College of Engineering, Mathematics and Physical Sciences,
University of Exeter, Harrison Building, North Park Road,
Exeter EX4 4QF, UK

M. J. Webb
Met Office Hadley Centre, FitzRoy Road, Exeter EX1 3PB, UK

Evidence for the low importance of thermal inertia comes in the form of φ having similar values in simulations of both transient and equilibrium climate change (Manabe et al. 1991). Not only that, but φ is approximately time-invariant in simulations of transient change in the twenty-first century despite rapid increases in forcing and land response over this period (JGW08). Coupled Model Inter-comparison Project 3 (hence CMIP3) climate model simulations of this period show φ lying between 1.3 and 1.8 (JGW08), and changing with time in any given model by 0.1–0.2 (JGW08). More idealised modelling work suggests a value for φ of approximately 1.4 (Byrne and O’Gorman 2013). In addition, φ has been shown to be invariant under very different CO₂ forcing amplitudes (Huntingford and Cox 2000).

The magnitude of φ in models is broadly consistent with observations of the last 30 years, although close comparisons are made difficult by internal variability in observations (Drost et al. 2012), and φ differing amongst the models. In addition, evidence mostly from simulations suggests that φ has increased from the mid twentieth century into the early twenty-first century: this is expanded on later in this section.

Differences in surface properties between land and ocean have been implicated in maintaining $\varphi > 1$ under climate change. The ocean can evaporate more effectively than land, thus inhibiting warming more than on land (Manabe et al. 1991; Sutton et al. 2007). JGW08 showed that the land–sea warming contrast was confined to the BL. They suggested that under a climate forcing, which in their case was perturbed sea surface temperature (henceforth SST), the lapse rate changed by more in the oceanic BL than in the land BL because relative humidity (henceforth RH) was on average larger over the ocean. In other words, while the BL lapse rate became more stable over both ocean and land as a result of the SST perturbation, the degree of stabilization was greater over the ocean. The temperature change in the lower free troposphere (henceforth LFT) just above the BL, i.e.: at a pressure of 600–700 hPa, was then similar over land and ocean. Such a model is shown as a schematic in Fig. 1, which shows a land–ocean warming contrast given a warming of the lower-free troposphere (T'_{LFT}) that is spatially uniform. The lapse rate changes less over land, where average RH is lower.

The magnitude of φ depends on multiple surface properties. Under a warming climate for instance, soil drying and a decrease in BL RH occurs where soil moisture is limited and evaporation is restricted by available moisture (Manabe et al. 1991, JGW08). In other words the local warming is a function of soil moisture as well as changes in soil moisture under climate warming. This can lead to less low-level cloud over land, which causes further land

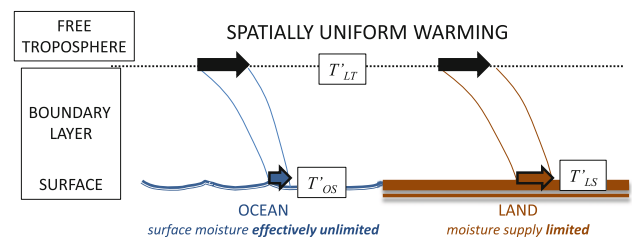


Fig. 1 Schematic of the conditions that bring about a land–sea warming contrast, i.e. $\varphi > 1$: the lower free troposphere warms by the same amount over land and ocean, which we denote in this idealised situation as T'_{LFT} , but the boundary layer over land and ocean warm differently, resulting in a larger land surface change than ocean surface change ($T'_{LS} > T'_{OS}$). The difference in surface constraints such as available moisture (and hence evaporative fluxes and average BL relative humidity) between land and ocean are also important contributors to the land–ocean difference

warming (JGW08, Fasullo 2010; Doutriaux-Boucher et al. 2009). Such a mechanism is similar to the summer drying phenomenon projected in models of midlatitude regions (Rowell and Jones 2006). In addition, at higher latitudes, changes in snow cover can play a role in changing the magnitude of land warming (Groisman et al. 1994). Physiological effects associated with CO₂ changes can also play a role in determining φ (Joshi and Gregory 2008): the physiological and radiative forcing associated with CO₂ changes would be expected to affect φ differently to methane for example, which only causes a radiative forcing. Changes to mid-tropospheric RH can also affect φ (Dommenges and Flöter 2011).

Climate model simulations suggest that when spatially varying forcing agents such as aerosols form a significant fraction of climate forcing and response, as happened in the middle-to-late twentieth century (Boucher and Lohmann 1995; Shindell and Faluvegi 2009), φ might be very different (Williams et al. 2000). Figure 2 shows φ plotted versus near-surface atmospheric temperature change (ΔT_{sa}) in 16 CMIP5 climate models being used for the UN Intergovernmental Panel on Climate Change’s 5th assessment report (IPCC AR5). The models are identified in Table 2. The top panel shows φ in integrations forced by all historic forcings, i.e. well-mixed greenhouse gases, stratospheric and tropospheric O₃, natural and anthropogenic aerosols, solar forcing and land use changes, whereas the bottom panel shows integrations conducted with CO₂ forcing only, which steadily increases at a rate of 1 % per year.

In both panels the intermodel and decadal spread in φ is very large when $\Delta T_{sa} < 0.2$ K, because φ is a ratio, and variability in the denominator (ocean temperature change) dominates when ΔT_{sa} is very small. In both panels the spread in φ narrows when ΔT_{sa} exceeds 0.7 K, being in the range 1.1–1.7 in the top panel, consistent with observations

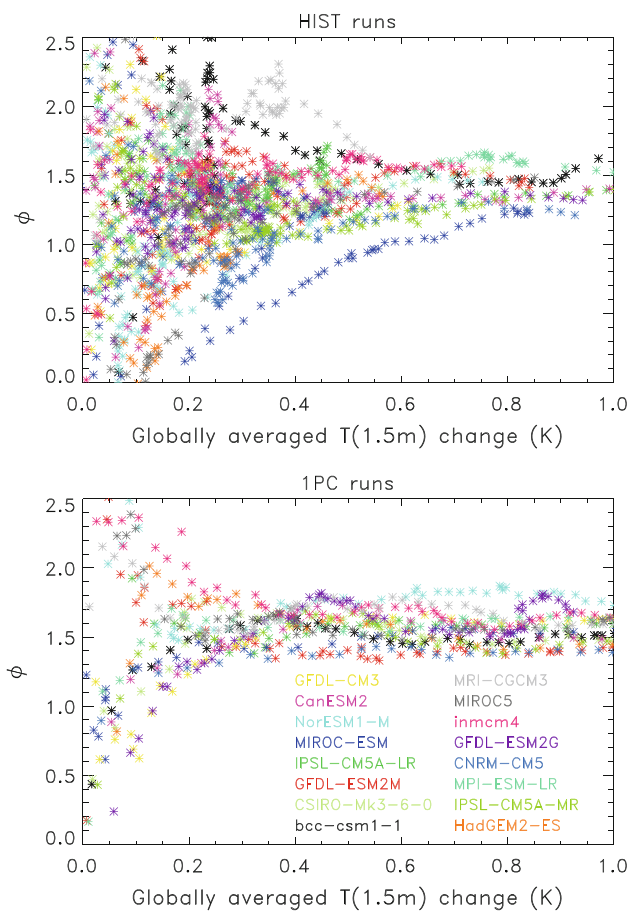


Fig. 2 *Top panel:* ϕ in 16 different CMIP5 climate models versus 1.5 m temperature change in integrations with historic forcings (well mixed greenhouse gases, natural and anthropogenic aerosols, solar variability) starting from 1860 until 2000. *Bottom panel:* as in the *top panel* but for integrations that are forced with CO₂ only increasing at a rate of 1 % per year

(Drost et al. 2012) and CMIP3 models (Sutton et al. 2007), but slightly higher (1.4–1.9) in the bottom panel.

However, the two panels differ somewhat in their spreads in ϕ when $0.2 < \Delta T_{sa} < 0.5$ K. Here the inter-model and decadal spread in ϕ in the “1%/year” runs (bottom panel) is small, suggesting that the large spread in ϕ in the “historic” forcings runs (top panel) is not associated with ΔT_{sa} being small. The difference is consistent with the response to aerosol forcing in the “historic” integrations: the forcing is not only significant compared to the well-mixed greenhouse gas forcing, but varies widely in magnitude amongst CMIP3 models (Forster et al. 2007).

In this paper we show in an illustrative conceptual model why ϕ should remain time-invariant to zeroth order under a range of twenty-first century transient warming and equilibrium scenarios, and yet be significantly different in simulations of the mid-twentieth century. We then test the conceptual model against integrations of two global circulation climate models, and discuss under what radiative

forcing scenarios ϕ should stay approximately unchanged for a given realisation or model. We also show how the conceptual model can shed light on how surface contrasts between land and ocean act in tandem with BL contrasts between land and ocean to give rise to a climate response that is global in nature, but amplified over the land surface.

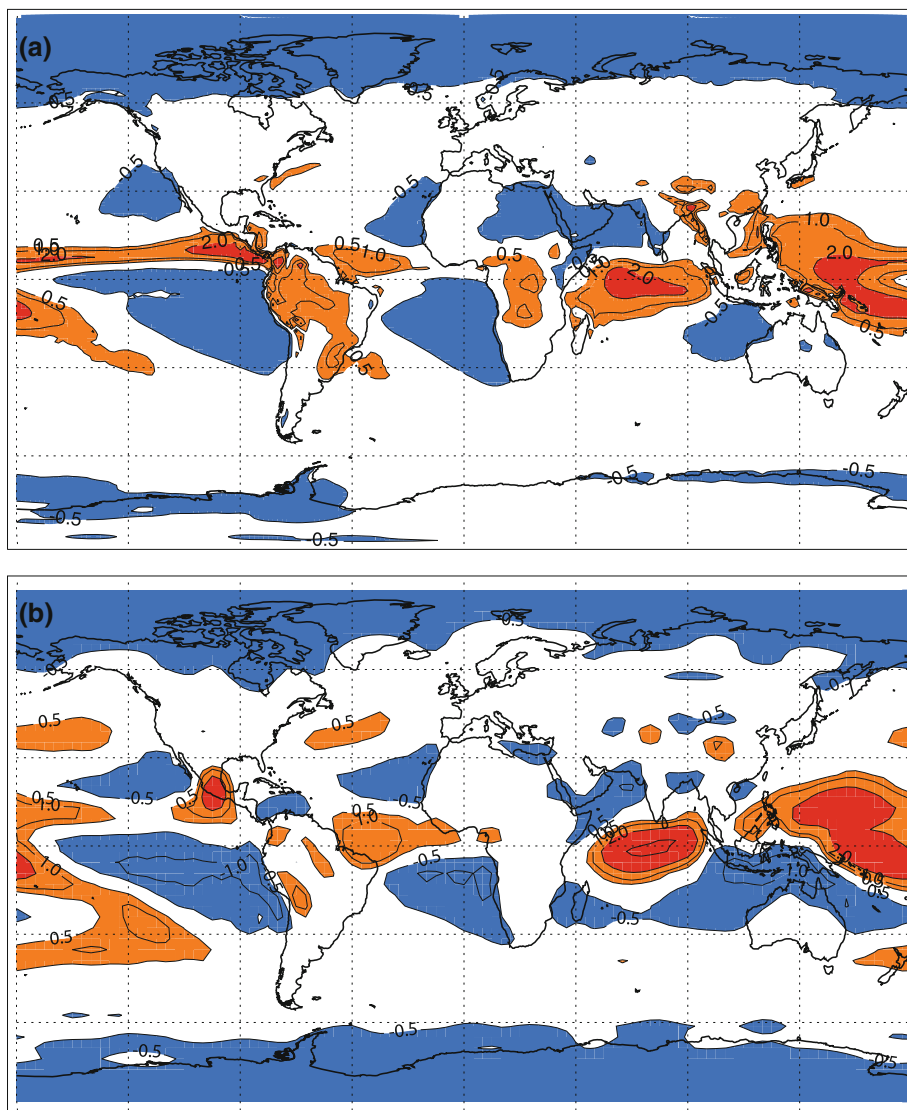
We use the conceptual model of JGW08 as a basis for the present work by stating the problem as follows: (a) what is the relationship between the spatial distribution of forcing and the spatial distribution of LFT warming; (b) under what LFT warming should the assumption of constant BL/surface amplification hold. Understanding both (a) and (b) enables constraints to be placed on the range of forcings under which ϕ remains approximately time-invariant to within 0.1–0.2 (c.f. JGW08 Fig. 3). Again it is stressed that the value of ϕ is invariably significantly greater than unity for spatially uniform forcings (Huntingford and Cox 2000, JGW08), and varies significantly between models (see Fig. 2).

Two models are chosen for the analysis: the IGCM (Intermediate Global Circulation Model) and HadGEM2a (Hadley Centre Global Environmental Model 2). The IGCM is similar to that of Cnossen et al. (2011), except the model is integrated with a horizontal resolution of T31 (approximately 3.75°) with 20 layers in the vertical. The IGCM is run in a “slab ocean” configuration (Forster et al. 2000), and integrations are carried out by adding different forcings with different magnitudes and spatial characteristics to the surface energy balance in order to warm the climate. HadGEM2 (Martin et al. 2011) is a state-of-the-art climate model, which is integrated using observed SSTs from 1978 to 2000 in the manner of the AMIP ensemble, as well as observed SSTs with 4 K added everywhere (Taylor et al. 2012). Although it is integrated with SSTs prescribed from observations, and is therefore not a fully coupled ocean–atmosphere climate model, its high vertical resolution in the BL makes it suited for the study in Sect. 4, because the study is concerned with analysing BL behaviour in the presence of a land–ocean surface warming contrast, which the HadGEM2 setup readily produces (JGW08).

2 Lower tropospheric warming: a conceptual model

The magnitude of the annually averaged diabatic heating in the atmosphere varies from about -1 to 2.5 K/day, with largest positive values in tropical regions where convection and heating by condensation is important: Fig. 3 shows such a pattern of diabatic heating or Q_{NET} in the IGCM and HadGEM2 climate models, averaged over the depth of the atmosphere down to the 700 hPa level (i.e. just above the BL). Both GCMs display heating in

Fig. 3 *Top panel:* diabatic heating pattern Q_{NET} ($K \text{ day}^{-1}$) in control integrations of the IGCM carried out under pre-industrial conditions. *Bottom panel:* the same pattern for HadGEM2, carried out using observed sea surface temperatures (SSTs). In both plots the contour interval is nonlinear ($-10, -5, -2, 1, -0.5, 0, 0.5, 1, 2, 5, 10$) to show up regions with smaller Q_{NET} than the convective regions



the tropical convective regions, and cooling in the subtropics and higher latitudes. In the time-mean, this pattern is balanced by advection, which leads to a smooth LFT temperature field in HadGEM2, as shown in Fig. 4 (top). The mixing is efficient in the zonal direction, as shown in Fig. 4 (bottom), which shows temperature with the zonal average removed: here anomalies are $O(1 \text{ K})$, and not significantly correlated with the land/ocean boundaries. The IGCM displays a similar temperature distribution (not shown).

The relatively smooth LFT temperature field of Fig. 4 suggests that the temperature response at LFT to a small heating perturbation (henceforth denoted Q') might also be smooth. Conversely, if gradients in Q' are large enough, atmospheric dynamics may not be able to produce a smooth temperature response at level LFT, causing a spatial anomaly there. If such an anomaly is

communicated to the surface, the potential exists for spatial anomalies in the surface temperature response to Q' as well. We note that “smooth” in this context means gradients that are small over continental scales rather than the hemispheric scale of the polar amplification signal (e.g.: Lu and Cai 2010).

We explore the above argument in two ways: firstly by employing a simple model framework; secondly by using a full GCM. The simple framework assumes that the net radiative heating at level LFT is smoothed in the horizontal by diffusive horizontal heat transport, and mainly directed zonally. We use this framework rather than the more conventional approach of modelling the evolution of temperature in the atmosphere as a whole, which is forced by the divergence of fluxes between the top of the atmosphere and the surface (e.g. North 1975), because we wish to simulate the temperature at level LFT, rather than the

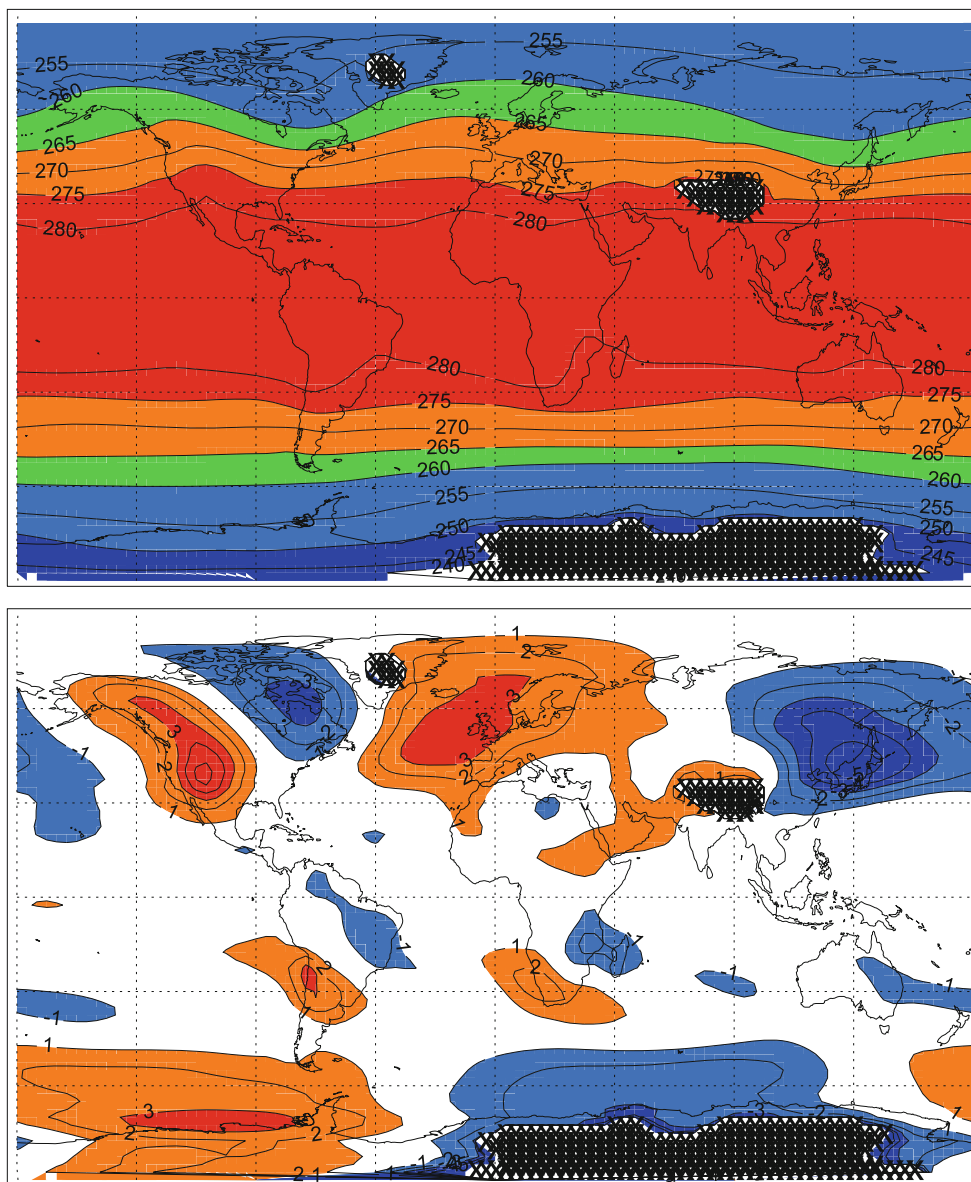


Fig. 4 *Top panel:* annually averaged temperature at the 700 hPa level in HadGEM2 (K). *Bottom panel:* temperature field with zonal average removed at the same level (K). Stippled areas are where the topography is higher than the 700 hPa level

average temperature in the whole atmospheric column or the temperature at the surface. In other words the conceptual model presented simply represents diabatic heating and the large scale advection of heat, rather than being a self-contained energy balance model in the manner of North (1975).

Large-scale meridional advection of heat has been represented using a simple diffusive form in simple energy balance models by North (1975), North et al. (1981), and Hwang and Frierson (2010). We start with a two-dimensional diffusive formulation, but concentrate on the zonal advection of heat for simplicity, as we wish to illustrate simply how horizontal heat transport modifies the response

to heating anomalies at level LFT. The evolution of temperature in the model atmosphere is then:

$$\partial T_{LFT} / \partial t = \alpha \nabla^2 T_{LFT} + Q_{NET} \tag{1}$$

where Q_{NET} is the net diabatic heating of the free atmosphere (in $K \text{ day}^{-1}$), and α is an effective thermal diffusivity (in $m^2 \text{ day}^{-1}$) that gives rise to the observed pattern of T_{LFT} . Physically Eq. (1) implies that net vertical fluxes into level LFT are manifested in Q_{NET} , and then mixed in the horizontal by large-scale advective motions. In general, α is $\alpha(x,y)$, and advective mixing tends to be more efficient in the zonal than meridional direction because of stronger zonal winds. The spatial distribution of

surface or in situ radiative forcing may be very different to the resulting pattern in the diabatic heating pattern. As an example, Fig. 3 shows that the Q_{NET} pattern associated with the relatively smooth net climatological solar forcing and infra-red cooling pattern has much spatial structure, mostly associated with convective heating and rainfall in the tropics. At equilibrium, averaging (1) in time gives:

$$\alpha \nabla^2 T_{LFT} = -Q_{NET} \quad (2)$$

In a similar way, one can consider what happens when a perturbation is added to the system, leading to an equilibrium response in T_{LFT} which we defined above as T'_{LFT} :

$$\alpha \nabla^2 T'_{LFT} - \beta T'_{LFT} + R' = 0 \quad (3)$$

Here the net diabatic heating perturbation Q' has been split into two parts: R' , which is the imposed climatic perturbation expressed as a heating rate (K day^{-1}), and $-\beta T'_{LFT}$, which represents the diabatic climatic response at level LFT (β has units of day^{-1}), and is proportional to the temperature perturbation T'_{LFT} . The LFT response arises as a result of a number of types of forcing. An increase in CO_2 directly changes tropospheric emission to space and hence the tropospheric heating rate. On the other hand, forcings which are felt mostly at the surface, such as solar forcing, have little direct impact on the atmosphere, mostly changing surface temperature. However, such surface changes are efficiently communicated vertically to LFT and then horizontally by convection and large-scale dynamics, respectively.

We assume that β is constant, i.e. the response is assumed to be proportional to T'_{LFT} for the radiative forcings considered here, in a similar manner to North (1975) and Budyko (1969). Because $\alpha \nabla^2 T'_{LFT}$ averages to zero in the global mean, the globally averaged values of R' and $\beta T'_{LFT}$ must equal each other. In general, α and β are functions of longitude and latitude. We assume that under climate change, α does not change (i.e.: there is no α' term). Such an assumption is consistent with other simple models of climate that represent the large-scale circulation by diffusive processes (e.g. North et al. 1981; Weaver et al. 2001).

One way to add significant spatial structure to T'_{LFT} is if R' has significant structure on small length scales sufficient to induce a response in $\alpha \nabla^2 T'_{LFT}$. The physical interpretation of this is that the atmospheric circulation is unable to mix the gradients in T'_{LFT} caused by the spatial variations in R' . Note that Eq. (3) implies that the response of T'_{LFT} to R' is a pattern that is smeared out in space compared with the pattern of R' itself, which is indeed the case with some of the idealised forcings studied by Forster et al. (2000), or twentieth century anthropogenic tropospheric aerosol forcing (e.g. Williams et al. 2000).

As a simple one-dimensional example of the above, consider the forcing $R' = \delta + \gamma \sin(\mu x)$, where the units of

δ and γ are K day^{-1} , and x is longitude in radians. The form of R' here is chosen to be roughly similar in scale to spatially confined forcings resulting from sulphate aerosol, and yet be analytically solvable. Here μ is an effective wavenumber that sets the spatial scale of the radiative perturbation. When this function is entered into (3) above, the solution is:

$$T'_{LFT} = (\delta/\beta) + \gamma \sin(\mu x)/(\beta + \alpha\mu^2), \quad (4)$$

while the heating perturbation Q' , or $R' - \beta T'_{LFT}$ (from Eq. 3) is given by

$$Q' = \gamma \sin(\mu x)(1 - \beta/(\beta + \alpha\mu^2)). \quad (5)$$

If R' is globally uniform, then $\gamma = 0$, and $T'_{LFT} = \delta/\beta$, i.e. proportional to the heating R' , but dampened by β . Q' is zero everywhere, consistent with $\nabla^2 T'_{LFT}$ being zero. As γ increases, the magnitude of the spatial gradient in R' becomes larger, as does the magnitude of Q' , and the spatial gradients in T'_{LFT} . Note that the magnitude of Q' is dependent on the magnitude of gradients in R' . On the other hand, as μ increases, i.e. the spatial scale of R' decreases, anomalies in T'_{LFT} are then damped by an amount dependent on the mixing term α .

We now speculate what values of γ , δ and μ might cause significant spatial anomalies in the pattern of T'_{LFT} at a given response length scale ΔL by scaling the equations above in a similar manner as e.g. Section 2.4 of Holton (1992). We assume for simplicity that $\gamma = \delta$, so that in some areas the local climate forcing can be zero, but not change sign, which is an idealised representation of the forcing distribution expected from aerosols (Kiehl et al. 2000). We also assume for simplicity that α and β are constant in space, and do not change when a radiative forcing is applied. Horizontal gradients in T'_{LFT} will approach the magnitude of the global mean response if the maximum value of the 2nd term of the RHS of (4) approaches the size of the 1st term. Since the maximum value of $\sin(\mu x)$ is unity, and $\gamma = \delta$, the 2nd term on the RHS of (4) approaches the size of the 1st term when $1/(\beta + \alpha\mu^2) \approx 1/\beta$. This is the case when:

$$\beta \approx \alpha\mu^2 \quad (6)$$

If (6) holds, then (5) implies that the magnitude of Q' must be $O(\gamma)$ in order for T'_{LFT} to exhibit significant spatial anomalies.

β can be estimated from considering variations in the mean state. If spatial variations in T_{LFT} have a scale of ΔL , the spatial derivative in Eq. (1) can be scaled to give $\Delta T_{LFT} \approx Q_{NET} \Delta L^2/\alpha$, or $\alpha \approx Q_{NET} \Delta L^2/\Delta T_{LFT}$, where ΔT_{LFT} is the magnitude of spatial variations in T_{LFT} . Replacing α in (6) gives $\beta \approx \mu^2 Q_{NET} \Delta L^2/\Delta T_{LFT}$, or:

$$\beta \Delta T_{LFT} \approx \mu^2 \Delta L^2 Q_{NET} \quad (7)$$

Given the assumption that β is constant in space, β can be substituted given that the globally averaged values of R' and $\beta T'_{LFT}$ are equal, i.e. $[R'] = [\beta T'_{LFT}]$ [see discussion following (3)]. The condition for horizontal gradients in T'_{LFT} becoming comparable to the magnitude of T'_{LFT} itself is then:

$$[R']\Delta T_{LFT}/[T'_{LFT}] \approx \mu^2 \Delta L^2 Q_{NET} \quad (8)$$

where the square brackets denote globally averaged values.

This is a potentially useful principle for determining if spatially varying climate forcings such as tropospheric aerosol can cause significant spatial variations in the pattern of T'_{LFT} . For instance, the climatological map shown in Fig. 4 (top panel) suggests that $\Delta T_{LFT} \approx 5$ K in the zonal direction over continental scales of 10^7 m. For twentieth century tropospheric aerosol forcing, $[T'_{LFT}]$ cools by ≈ 0.5 K (Mitchell and Johns 1997), so $\Delta T_{LFT}/[T'_{LFT}] \approx 10$. Aerosol forcing is mostly confined to the continents (e.g. Boucher and Lohmann 1995; Williams et al. 2000), while the response significantly extends over the oceans (Williams et al. 2000), so $\Delta L \approx 2x$ the wavelength λ of the forcing. Using the identity $\lambda = 2\pi/\mu$ gives $\mu^2 \Delta L^2 \approx 10$. Equation (8) then implies that the response in T'_{LFT} to twentieth century anthropogenic forcing will be inhomogeneous if $[R'] \approx Q_{NET}$.

Though R' for aerosol can exceed 1 K day^{-1} locally (Reddy et al. 2011), globally averaged values of $[R']$ are much lower. One can estimate $[R']$ by assuming that globally averaged heating scales with maximum local heating in a similar manner to the TOA radiative forcing F' . $F'_{max} \approx 10 [F']$ (Kiehl et al. 2000), which implies that in the global mean $[R'] \approx 0.1 \text{ K day}^{-1}$. This is an approximate analysis, but it suggests that twentieth century anthropogenic aerosol forcing could cause significant spatial anomalies in the resulting $[T'_{LFT}]$, and potentially alter φ , because, as shown in Fig. 3, climate models suggest that $Q_{NET} < 0.5 \text{ K day}^{-1}$ outside convective regions. Such a result suggests the potential for φ in CMIP5 twentieth century simulations to have different values to φ in simulations of the twenty-first century forced predominantly by well-mixed greenhouse gases, as hypothesised in the last section.

The conceptual model can point to a reason why twenty-first century and time-invariant CO_2 forcing lead to similar values of φ in climate models despite the presence of significant ocean heat uptake: the globally averaged surface flux associated with heat uptake is similar in magnitude to twentieth century tropospheric aerosol forcing (e.g. Raper et al. 2002), but mostly occurs on much larger spatial scales than twentieth century anthropogenic aerosol forcing. Anomalies in T'_{LFT} associated with heat uptake can therefore be effectively spread out spatially by the circulation,

leaving φ unchanged, which is consistent with the results of Lambert and Chiang (2007).

The conceptual model, while useful, does contain a number of simplifications, such as a spatially uniform α and β . While its findings for spatially varying forcings are compared to a GCM in the next section, limitations placed on it by the size of R' are now explored. Significant changes to the pattern of T'_{LFT} (and hence φ) might occur if R' is so large that either α changes significantly, or is so large that the linear $\beta T'_{LFT}$ approximation in (3) breaks down. A lower bound to a regime where the above changes might happen is already known, since φ has been shown to remain relatively constant for forcings up to and including when CO_2 is quadrupled from pre-industrial values (Huntingford and Cox 2000), i.e.: $F' \approx 7.5 \text{ Wm}^{-2}$ and $T'_{surface} \approx 6$ K. Using an energy balance framework model, Budyko (1969) suggest a much higher upper bound for the validity of a linear relationship between top-of-atmosphere radiation balance change and temperature of approximately 30 K. In the next section we investigate the effects of forcings $\leq 20 \text{ Wm}^{-2}$ using the IGCM in order to assess if the assumptions of the above conceptual model become invalid under values of T'_{LFT} of 5–20 K.

3 Lower tropospheric warming: IGCM simulations

We now examine $Q' = R' - \beta T'_{LFT}$ (from Eq. 3) and T'_{LFT} in a series of integrations of the Reading IGCM using idealised forcings (which are summarised in Table 1) in order to evaluate the conceptual model and its predictions. Figure 5 shows Q' in run 5G, which has globally uniform surface forcing of magnitude 5 Wm^{-2} . Despite the heating perturbation R' being spatially uniform, the pattern of Q' is similar to the pattern of Q_{NET} , in that there is heating over the Western Pacific and equatorial oceans, and cooling in the subtropics. The only noticeable difference is in the equatorial Indian Ocean, associated with a changed monsoonal circulation in the warmer 5G world. The overall magnitude of the pattern of Q' is about 1/5 the size of Q_{NET} .

Figure 6a shows the geographical difference in Q' between a run with forcing that is constrained meridionally in the northern hemisphere (denoted 5N) and a run with forcing that is globally constant (denoted 5G). Figure 6b shows the same thing, but for a forcing that is constrained zonally in the western hemisphere (denoted 5W). Comparing Fig. 6a with b shows that the difference in Q' between a run with meridionally constrained forcing (run 5N) and a run with globally constant forcing (run 5G) is much larger than the difference in Q' between a run with zonally constrained forcing (run 5W) and a run with globally constant forcing (run 5G).

Table 1 Model runs, type of surface forcing, and land–sea surface warming ratio φ

Run	Surface forcing condition and model	φ
C	Control integration, IGCM	–
5N	10 Wm ⁻² applied to N hemisphere (global 5 Wm ⁻²), IGCM	1.81
5S	10 Wm ⁻² applied to S hemisphere (global 5 Wm ⁻²), IGCM	0.89
5E	10 Wm ⁻² applied to E hemisphere (global 5 Wm ⁻²), IGCM	1.33
5W	10 Wm ⁻² applied to W hemisphere (global 5 Wm ⁻²), IGCM	1.20
L1	10 Wm ⁻² applied to 40°E–120°E, 20°N–60°N, IGCM	2.48
L2	20 Wm ⁻² applied to 40°E–120°E, 20°N–60°N, IGCM	2.40
O1	10 Wm ⁻² applied to 140°E–220°E, 20°N–60°N, IGCM	1.81
O2	20 Wm ⁻² applied to 140°E–220°E, 20°N–60°N, IGCM	1.71
5G	5 Wm ⁻² applied globally, IGCM	1.26
10G	10 Wm ⁻² applied globally, IGCM	1.29
15G	15 Wm ⁻² applied globally, IGCM	1.30
20G	20 Wm ⁻² applied globally, IGCM	1.32
H	HadGEM2 integration with AMIP sea surface temperature	–
H4K	As H but with 4K added to sea surface temperature	1.42

Table 2 CMIP5 models used in this paper

Modeling center (or Group)	Institute ID	Model name
Beijing Climate Center, China Meteorological Administration	BCC	BCC-CSM1.1
College of Global Change and Earth System Science, Beijing Normal University	GCESS	BNU-ESM
Canadian Centre for Climate Modelling and Analysis	CCCMA	CanESM2
Centre National de Recherches Meteorologiques/Centre Europeen de Recherche et Formation Avancees en Calcul Scientifique	CNRM-CERFACS	CNRM-CM5
Commonwealth Scientific and Industrial Research Organization in collaboration with Queensland Climate Change Centre of Excellence	CSIRO-QCCCE	CSIRO-Mk3.6.0
NOAA Geophysical Fluid Dynamics Laboratory	NOAA GFDL	GFDL-CM3 GFDL-ESM2G GFDL-ESM2M
Met Office Hadley Centre	MOHC	HadGEM2-ES
Institute for Numerical Mathematics	INM	INM-CM4
Institut Pierre-Simon Laplace	IPSL	IPSL-CM5A-LR IPSL-CM5A-MR
Japan Agency for Marine-Earth Science and Technology, Atmosphere and Ocean Research Institute (The University of Tokyo), and National Institute for Environmental Studies	MIROC	MIROC-ESM
Atmosphere and Ocean Research Institute (The University of Tokyo), National Institute for Environmental Studies, and Japan Agency for Marine-Earth Science and Technology	MIROC	MIROC5
Max Planck Institute for Meteorology	MPI-M	MPI-ESM-LR
Meteorological Research Institute	MRI	MRI-CGCM3
Norwegian Climate Centre	NCC	NorESM1-M

The maximum difference in the magnitude of Q' between 5N and 5G is about 0.5 K day⁻¹ (see Fig. 6a), which is approaching the size of Q_{NET} , which is about 1–2 K day⁻¹ (see Fig. 3). The conceptual model of the last section suggests that run 5N might exhibit spatial anomalies in T'_{LFT} . This indeed is the case as shown in Fig. 6c, which shows that T'_{LFT} in run 5N, when normalised by the

response in 5G, is much larger than unity in the northern hemisphere, but much smaller than unity in the southern hemisphere. By comparison, T'_{LFT} in 5W, when normalised by run 5G, is near unity almost everywhere, as shown in Fig. 6d.

The temperature response in 5N compared to 5G suggest that the heating anomaly Q' in run 5N is not mixed

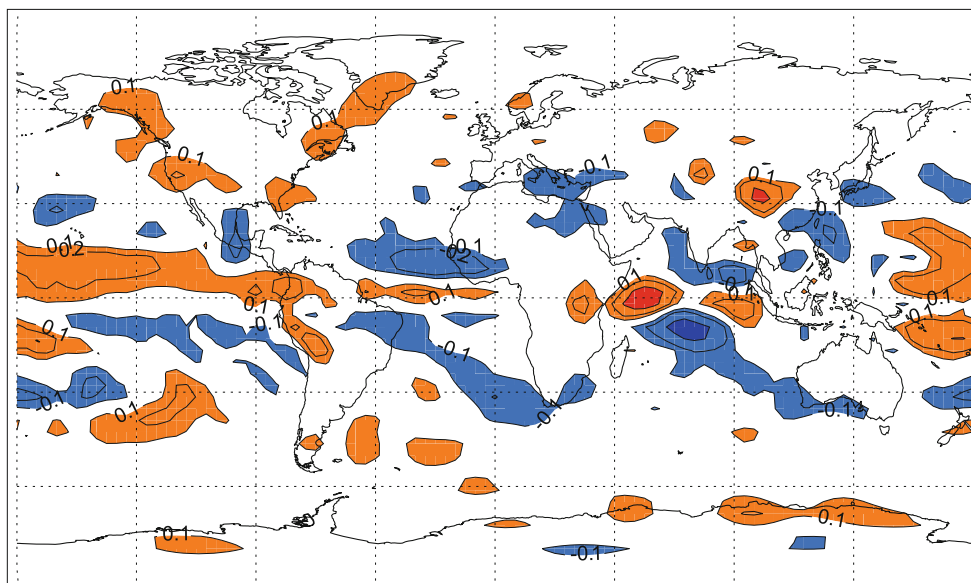


Fig. 5 Diabatic heating perturbation Q' in run 5G (K day^{-1}). The contour intervals are the nonlinear intervals of Fig. 3 but multiplied by 0.2, to show up regions with smaller Q' than the convective regions

efficiently in the meridional direction. Conversely, Q' in run 5W is mixed efficiently in the zonal direction, leading to a smaller difference in T'_{LFT} between 5W and 5G. The results shown above are symptomatic of the meridional atmospheric circulation not being able to transport enough heat across the equator to compensate for the asymmetry in the forcings in run 5N. This is consistent with previous work performed using GCMs (Williams et al. 2000; Yoshimori and Broccoli 2008; Shindell et al. 2010), and does point out a limitation of the conceptual model of the last section, which did not account for directional differences in heat transport.

Table 1 shows that the above results are reflected in φ : run 5W, and another run 5E, which has forcing restricted to the Eastern hemisphere, both exhibit values of φ that are similar to run 5G to within $O(0.1)$: conversely values of φ in run 5N, and another run 5S, which has forcing restricted to the southern hemisphere, are very different. This difference is due to the climate response in run 5N being confined to the northern hemisphere, which has a high proportion of land coverage, and vice versa in run 5S. These results suggest that hemispheric-scale forcings that vary zonally cause changes in φ that are smaller than forcings that vary meridionally. Twentieth century aerosol forcing lies in between these two paradigms (e.g. Boucher and Lohmann 1995), and indeed the CMIP5 ensemble simulations of the twentieth century suggest that φ varies by 0.1–0.5 in simulations forced by aerosol, as shown in the top panel of Fig. 2.

Equation 8 and the subsequent discussion suggest that the ability of spatially confined forcings to affect φ depends on their spatial scale, so the effect of forcings

confined to sub-continental regions (such as twentieth century black carbon forcing) is now considered. Figure 7 shows zonally averaged Q' and T'_{LFT} in runs O1 and L1, which are imposed forcings over parts of the ocean and land, respectively (see Table 1). The forcing is large enough to cause a significant spatial anomaly in Q' which is different in character in runs O1 and L1, with the latter having a much greater local response. Some of the localisation is due to a change in Q' forced by a South Asian monsoon-like response (not shown). Figure 7c, d shows that the patterns of T'_{LFT} in runs L1 and O1 are more spatially uniform than Q' , because Q' is related to $\nabla^2 T'_{LFT}$ rather than T'_{LFT} , consistent with the smoothing behaviour of the conceptual model of the last section.

The value of φ in O1 is 1.81, which is similar to the value φ of in run 5N (see Table 1). This is likely to be because the forcing in O1 is confined to the northern hemisphere, as is the forcing in run 5N, so the response in O1 is also confined to the northern hemisphere; because the northern hemisphere has more land, φ has a high value. φ in run L1 is 2.48, which is even higher than its value in O1, because even though the climate responses are smoothed versions of the forcings, the T'_{LFT} responses are by no means zonally uniform, as shown in Fig. 7c, d. A forcing over the land is therefore felt more over the land than the ocean (and vice versa), which is reflected in the high value of φ in run L1 compared to O1.

Runs O1 and L1 can be compared with integrations O2 and L2, which are structurally similar, but both have twice the forcing magnitudes of O1 and L1 respectively. Table 1 shows that φ has similar values in runs O1 and O2 (1.8 and 1.7), and runs L1 and L2 (2.4 and 2.5), confirming the

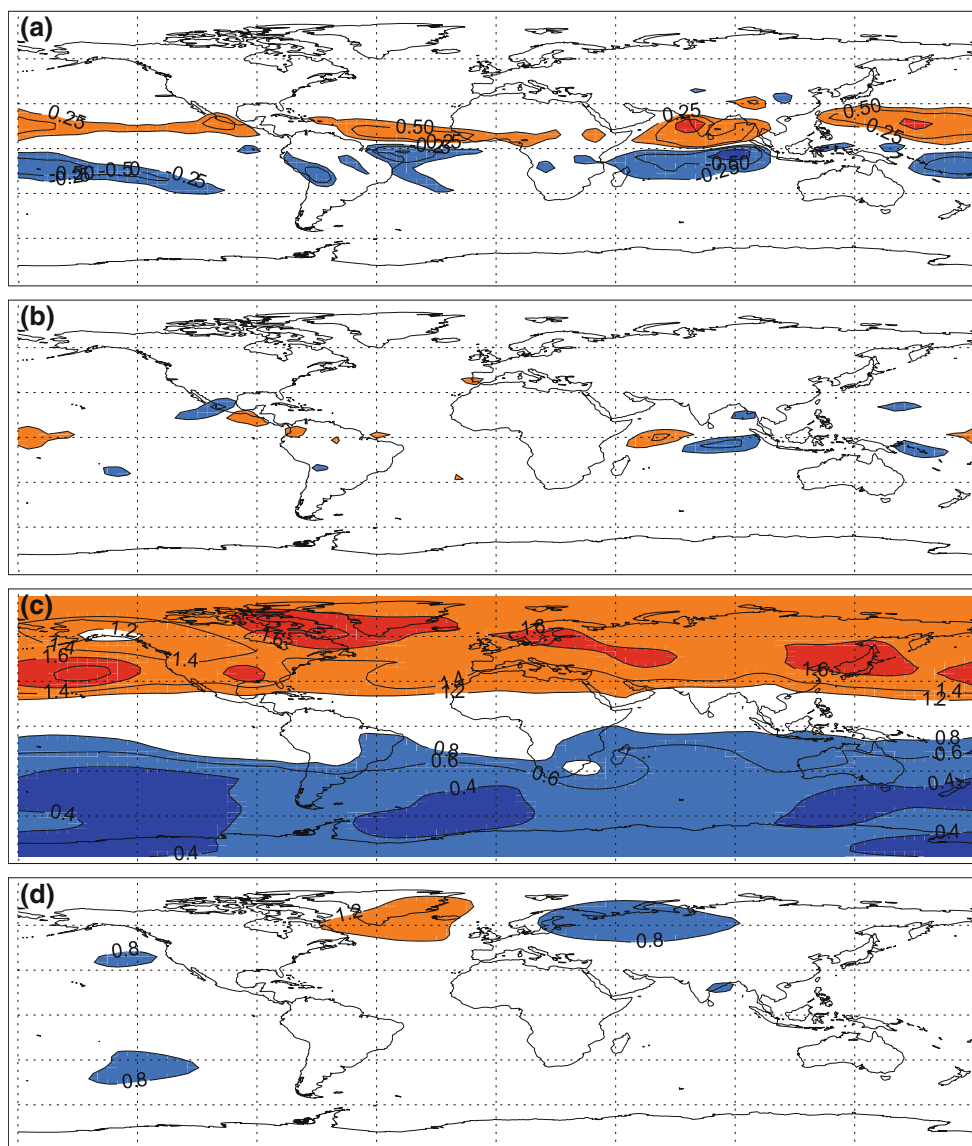


Fig. 6 **a** Difference in diabatic heating perturbation Q' between 5N and 5G; **b** difference in Q' between 5W and 5G; **c** T'_{LFT} pattern in 5N normalised by T'_{LFT} in 5G (both compared to C); **d** T'_{LFT} pattern in 5W normalised by T'_{LFT} in 5G (both compared to C). The contour intervals

in (a) and (b) are the same nonlinear intervals as the nonlinear intervals of Fig. 3 but multiplied by 0.5, and linear for the temperature maps (c) and (d)

result of the conceptual model that φ is more dependent on forcing scale than on magnitude. In addition this result also shows that the insensitivity of φ to forcing magnitude found by Huntingford and Cox (2000) also applies to localised forcings of the scale of O1 and L1. Interestingly, the zonally averaged response to the forcing is independent of whether or not the forcing is over land or ocean: we comment on this in the next section.

We now consider the effect of very large geographically uniform surface forcings, having amplitudes of 10, 15 and 20 Wm^{-2} , denoted as 10G, 15G and 20G, respectively (see Table 1). For reference, quadrupling CO_2 from pre-

industrial values causes a forcing of approximately 7.5 Wm^{-2} . Because the forcings are globally uniform, we display zonal averages for clarity. The zonally averaged diabatic heating pattern is shown in Fig. 8a, which shows that Q' only approaches values comparable to Q_{NET} in runs 15G (grey solid) and 20G (grey stars). Consequently, T'_{LFT} , when normalised by T'_{LFT} in run 5G, does not significantly deviate from unity apart from over the Southern Ocean in any of the runs, as shown in Fig. 8c. This response is also mirrored in surface temperature, which shows normalised responses in all runs that are within 10 % of the response in 5G, again everywhere away from the Southern Ocean (see

Fig. 7 **a** Difference in diabatic heating perturbation Q' between O1 and C; **b** difference in Q' between L1 and C; **c** T'_{LFT} in O1 minus C; **d** T'_{LFT} in L1 minus C. In all cases the rectangular box marks the boundary of the aerosol forcing zone. The contour intervals are the same nonlinear intervals as in Fig. 5 for the diabatic heating maps (a) and (b), and linear for the temperature maps (c) and (d)

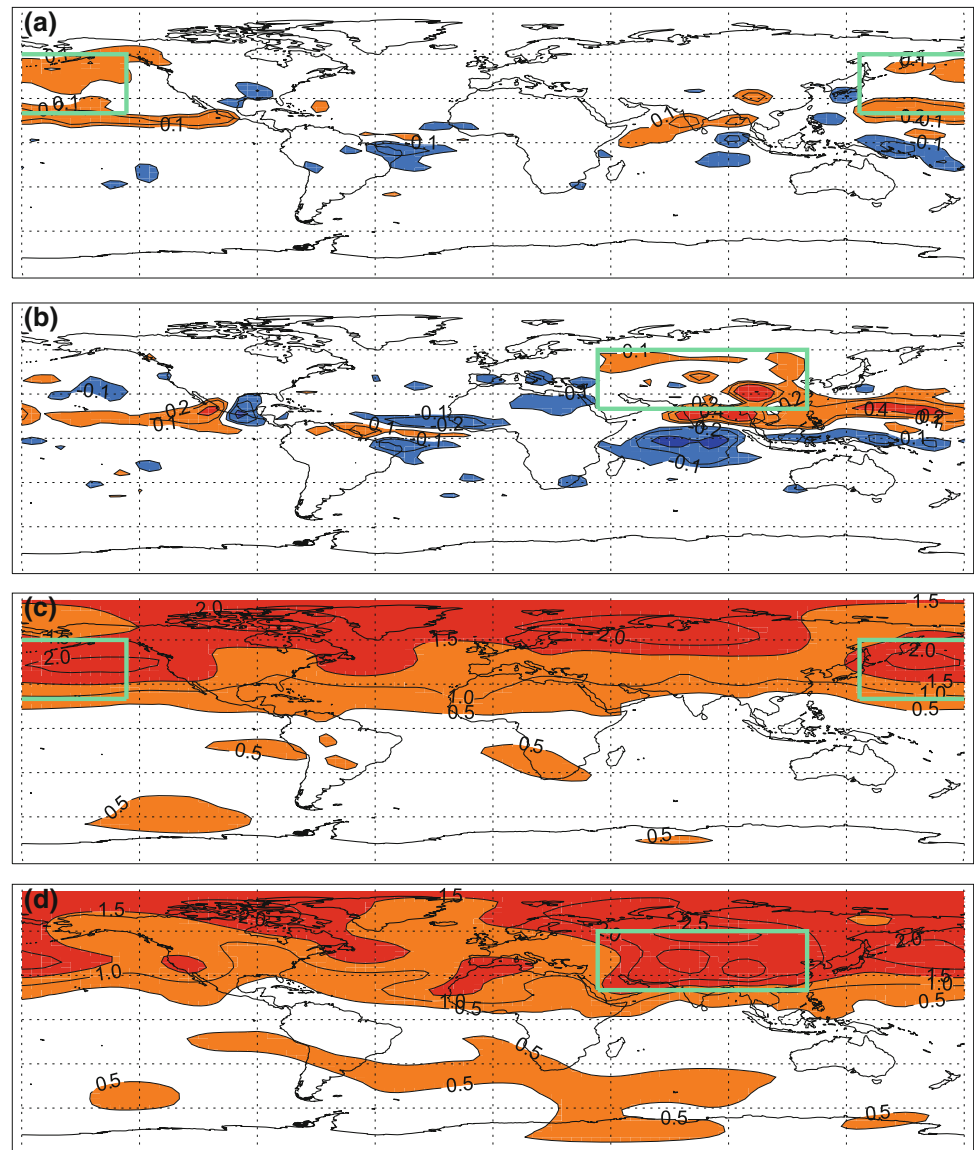


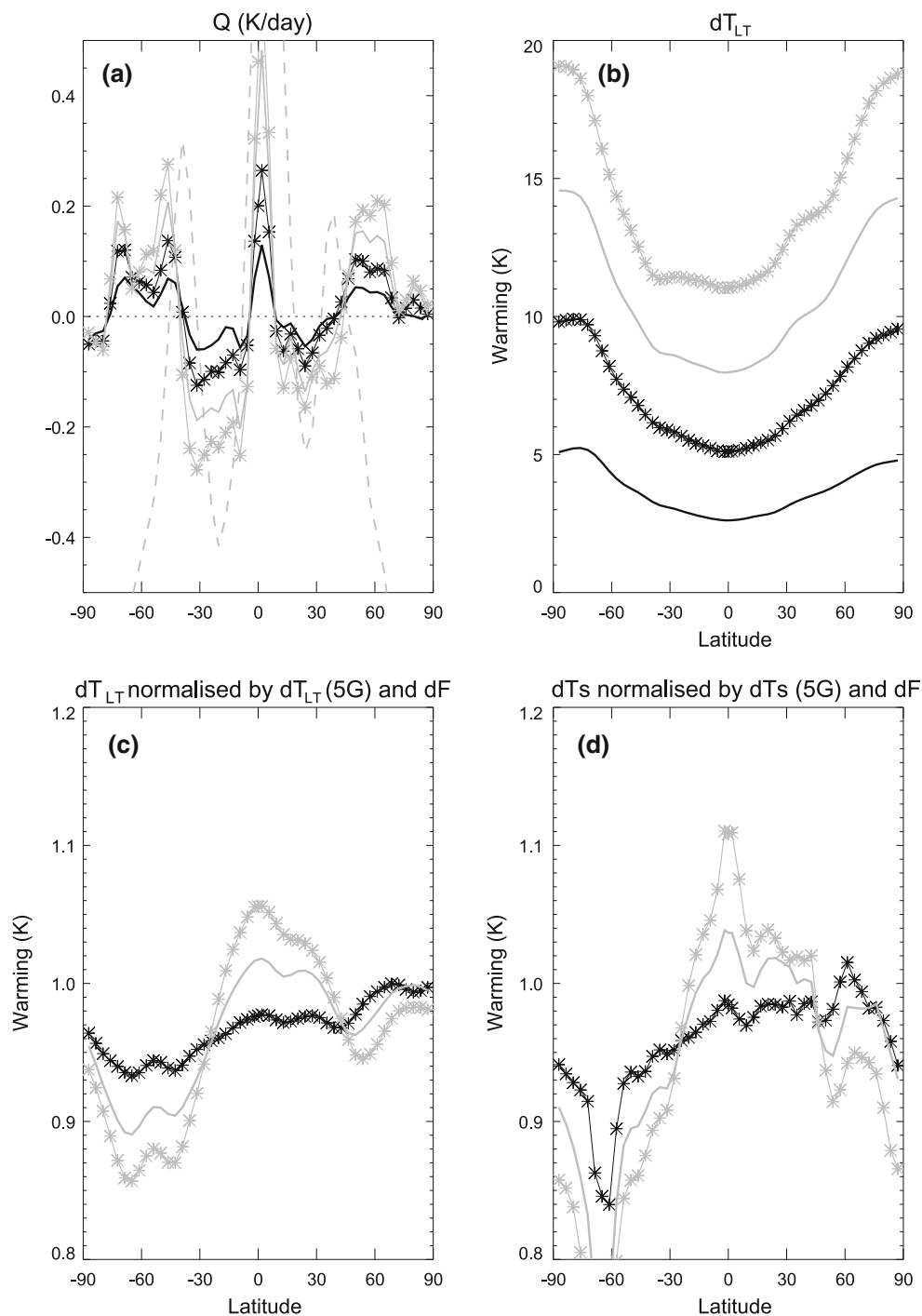
Fig. 8d). The nonlinearity over this region could be a result of nonlinearities in the sea-ice response (Forster et al. 2000).

The values of φ in runs 5G, 10G, 15G and 20G are within 10 % of each other (see Table 1), despite some differences in zonally-averaged T'_{LFT} response. This is because when averaging over area, the tropical and subtropical responses dominate the globally-averaged value of φ : Fig. 8 shows that over most latitudes the zonally averaged value of T'_{LFT} and surface temperature in run 20G lies within 10 % of its value in run 5G when normalised by the globally averaged change, leading to small differences in φ . The small differences in φ between runs 5G, 10G, 15G and 20G when compared to the difference in φ between runs O1 and L1 is commented on in Sect. 5.

4 Lower tropospheric and boundary layer warming: simulations with a full GCM

JGW08 showed that the area-averaged contrast in temperature and lapse rate change between land and ocean was confined to the lowest 3 km of the atmosphere in the HadGEM2 climate model, suggesting that the LFT level discussed in previous sections lies above this height. We now diagnose the height of the BL in more detail to establish the level of LFT. The HadGEM2 model is used because it has higher vertical resolution and more complexity in its BL representation than the IGCM. The runs examined here are denoted H and H4K (see Table 1). Although the experiments are carried out with fixed SSTs, the “+4K” run (H4K) exhibits a zonally uniform temperature change at LFT as well as a surface/BL land–sea

Fig. 8 **a** Zonally averaged diabatic heating perturbation Q' ; **b** T'_{LFT} pattern; **c** normalised T'_{LFT} pattern; **d** normalised T_s response in IGCM runs. In all cases run 5G is solid, 10G is stars, 15G is grey and 20G is grey stars. The normalised pattern for run XG in (c) and (d) has been divided by the 5G response, and by the ratio of the forcings in XG and 5G, i.e. $X/5$. The control Q_{NET} in the top left panel (a) is shown in dashed grey



warming contrast in a similar manner to JGW08, so is adequate for our purposes.

First we compare the magnitude of annually averaged heating from BL processes with that from explicit advection. The height where this quantity becomes small should be where advection dominates over BL processes, and is the “LFT” level of the conceptual model. Figure 9a shows that over the ocean, this condition is met at a height of ~ 2 km in the tropics, and ~ 3 –4 km in the extratropics,

suggesting that LFT lies at or above these heights over the ocean. Over land, Fig. 9b shows that the condition is met at a height of about 3–4 km, suggesting that LFT is at a height of approximately 3–4 km, or about 600–700 hPa.

Figure 9c shows the zonally averaged temperature difference between run H4K and run H over ocean points compared to the zonally averaged temperature difference. The difference is small above ~ 2 km in the tropics, and 3–4 km in the extratropics, and is consistent with the height

at which heating due to BL processes is small compared to heating due to advection (see Fig. 9a). Similarly, Fig. 9d shows amplification of a warming signal over land compared to the zonal mean up to approximately 3–4 km in height, which is consistent with Fig. 9b. These results suggest that LFT lies above 2 km in the tropics, and above 3–4 km in the midlatitudes.

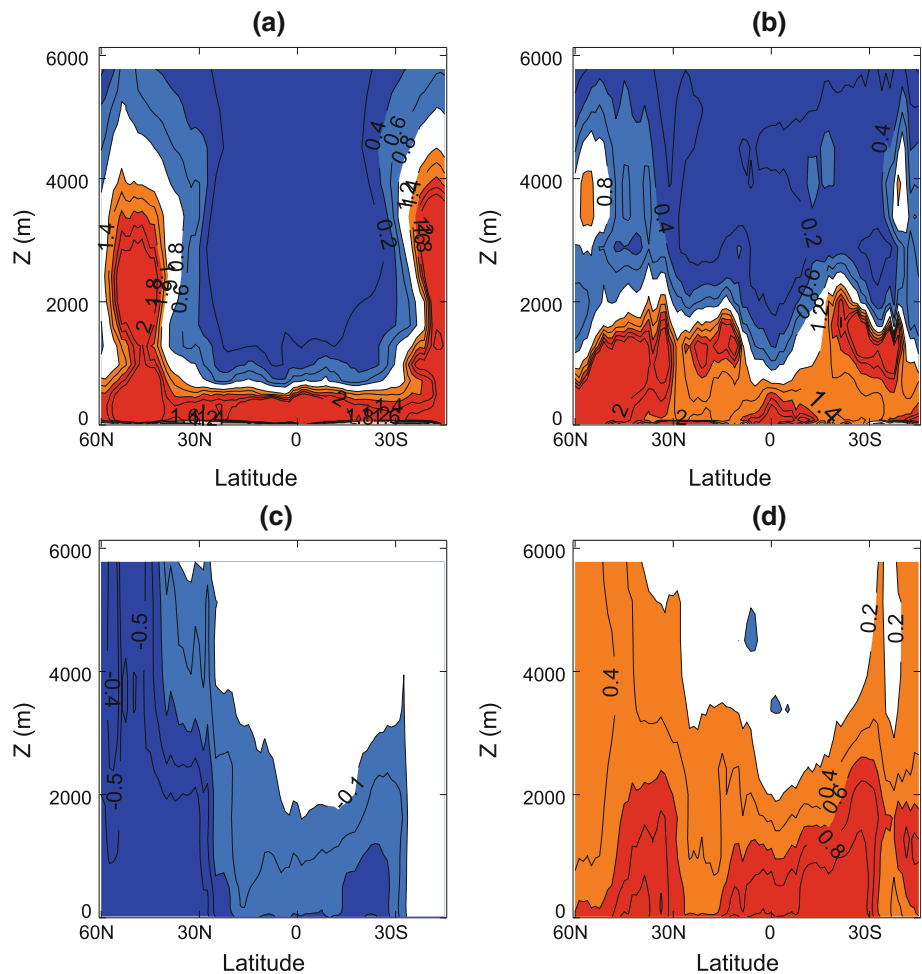
The arguments presented in the previous sections only imply an unchanged ϕ if the scaling from T'_{LFT} to land and ocean surface temperature change remains constant. Whether or not this happens depends on how BL RH and lapse rate change with temperature, which in turn is dependent on moisture availability and surface-atmosphere exchange properties such as evaporative fraction (e.g. Manabe et al. 1991, JGW08). While each of these quantities are related to each other, we shall examine the surface and atmospheric properties in turn to see if what magnitude of temperature change might change ϕ despite a spatially homogenous T'_{LFT} .

First, we consider the effect of BL RH: for instance taking the extreme example of a completely dry land BL, and a continually saturated ocean BL, the land lapse rate is

the dry lapse rate Γ_d while the ocean lapse rate is given by the saturated adiabat $\Gamma_d(1 + (L/C_p)dq_s/dT)$ (Holton 1992, equation 9.42). Quantifying this, the denominator in the saturated lapse rate above only changes by $\sim 10\%$ over 5 K. Given that many areas of the world lie well away from these two extremes, we expect that a climatic $T'_{LFT} \gg 5$ K is required for the changes in saturated lapse rate to cause significant changes in ϕ under climate change. Such a result is also consistent with the results of runs 5G, 10G, 15G and 20G as shown in Table 1.

Second, we consider the BL RH changes associated with moisture limitation above dry soils. This should not contribute to a significant change in ϕ because over the land as a whole the change in RH in the BL is small when doubling CO_2 , exceeding 10% over only a very small number of grid points (JGW08). The small change in RH suggests a small change in evaporative fraction with temperature, and hence a small change in ϕ as climate warms. Nonlinearities might also be expected to play a role in this part of the mechanism. As land warms and dries, evaporative fraction and BL RH decrease, and low cloud decreases, further warming the land surface. On the other hand once

Fig. 9 **a** Ratio of the magnitude of annually averaged heating (K day^{-1}) from the boundary layer physics to the magnitude of heating from advection in run HC: averaging is over ocean points only; **b** as in (a), but averaging over land points only; **c** The difference in annually averaged temperature change between run H4K and run H over ocean points only, as an anomaly from the zonally averaged difference (K); **d** as in (c) but for land points only. The contour intervals are 0.2 K day^{-1} in (a) and (b), 0.1 K in (c) and 0.2 K in (d)



evaporation approaches zero, as is typically the case for desert environments, increases in temperature are not amplified by further changes in evaporative fraction. In addition, because there is very little cloud in these regions, increases in temperature do not cause additional low cloud feedbacks (JGW08).

An exact determination of what climate forcing might lead to such nonlinear behaviour is beyond the scope of this paper since any such behaviour would be sensitive to the nature of the land surface scheme used in any given model. Indeed different models show different soil moisture responses to climate change (e.g. Lambert and Allen 2009). Nevertheless the results of runs 5G, 10G, 15G and 20G suggest that a change in T'_{LFT} well in excess of 10 K is needed before changes in φ become evident, which is much higher than most estimations of climate change over the next 2–3 centuries (e.g. Meehl et al. 2007, Figure 10.4). Such a conclusion is consistent with other research using idealised climate models having globally averaged values of T'_{LFT} exceeding 20 K (Byrne and O’Gorman 2013).

5 Discussion: regional-scale forcings

The condition for small spatial anomalies in T'_{LFT} is similar for both the conceptual model and the IGCM: that spatial variations in the imposed heating perturbation R' should be small, so that spatial anomalies in the resulting diabatic heating perturbation Q' are also small. The IGCM results suggest that “small” in this instance means that spatial variations in Q' should be smaller than spatial variations in the climatological Q_{NET} . Any spatial variation in R' will also cause a response in rainfall (e.g. Ackerley et al. 2011; Fasullo 2010), whose effects on soil moisture are not in the conceptual model, but will change φ (e.g. JGW08). Another caveat for the conceptual model is the difference between meridional and zonal transport magnitudes in a real GCM. Despite these caveats, the conceptual model is a useful tool for predicting what spatially varying forcings can cause changes to φ .

The conceptual and numerical model results can explain the difference in φ between climate simulations with a significant spatially varying anthropogenic aerosol component, such as the mid twentieth century (Boucher and Lohmann 1995; Shindell and Faluvegi 2009; Kiehl et al. 2000), and model projections forced predominantly by well mixed greenhouse gases (e.g. Mitchell and Johns 1997). Interestingly, while the zonal extent of T'_{LFT} associated with the “spatially restricted forcing over land” run L1 is less than that associated with the “spatially restricted forcing over ocean” run O1, the zonally and globally averaged values of T'_{LFT} associated with L1 and O1 are very similar. This suggests that climate sensitivity does not

depend on whether a given forcing occurs on land or ocean, consistent with previous work (Forster et al. 2000; Lambert et al. 2011).

It has been suggested that φ is affected by a collapse of the Atlantic meridional overturning circulation (AMOC). In this case a change in the heat uptake in the North Atlantic causes a large change in net flux at the surface, and a change in φ over large regions of Europe: indeed this has been demonstrated in a climate model (Laurian et al. 2010). The magnitude of the anomalous ocean surface heat flux is well over 30 Wm^{-2} , and gradients approach $1 \text{ Wm}^{-2} \text{ degree}^{-1}$ (Laurian et al. Figure 4), which is even larger than the O2 run, which implies significant anomalies in of Q' , T'_{LFT} , and hence φ .

Some geo-engineering strategies involve changing the properties of ocean clouds such that the globally averaged radiative forcing counteracts the warming effect of anthropogenic greenhouse gases. Some models of such strategies involve changing oceanic stratocumulus clouds (e.g. Jones et al. 2009). However, such regional changes are analogous to runs O1 or O2, in that the radiative forcing is concentrated in relatively small areas over the ocean, and indeed Jones et al. (2009) found a spatially confined near-surface air temperature response, consistent with our results.

Interestingly, other geoengineering studies involve changes over larger regions of the oceans. For instance, Bala et al. (2011) found a value of $\varphi \approx 1.1$ in an experiment forced by changes to all oceanic clouds, as opposed to $\varphi \approx 1.3$ in experiments in which CO_2 was doubled, suggesting that the oceanic forcing in Bala et al. (2011) lies on the edge of the regime in which φ is unchanged by efficient spatial mixing of temperature at level LFT .

The value of φ will be affected by land cover changes such as vegetation disturbance that occur under climate change which then affect surface characteristics such as evaporation, and moisture supply to the boundary layer. Even in the absence of land cover changes, physiological changes, such as those associated with CO_2 -induced stomatal conductance changes, will increase φ by restricting evaporation over forested areas (Joshi and Gregory 2008). The effects of physiological changes on restricting evaporation have been found to be in excess of 10 Wm^{-2} over large regions of South America and Africa in climate simulations in which CO_2 is quadrupled from pre-industrial values (Doutriaux-Boucher et al. 2009), which is consistent with experiment L1 showing that such changes are large enough to affect φ (see Table 1).

6 Discussion: continental and larger scale forcings

The above conceptual and numerical model results suggest why φ is approximately time-invariant in anthropogenically

forced transient change projections of the twenty-first century. The similarity in φ between runs 5E and 5W suggests that the flux into the ocean from transient heat uptake has to be much larger than the 10 Wm^{-2} peak forcing amplitude of 5E and 5W to cause a significant anomaly in T'_{LFT} . In climate model simulations, the flux associated with ocean heat uptake is only $1\text{--}4 \text{ Wm}^{-2}$ (e.g. Raper et al. 2002), so the land and ocean warm in tandem, and φ is nearly invariant in GCM simulations of transient twenty-first century change (Lambert and Chiang 2007, JGW08).

More locally, smaller regions such as the Labrador sea, Greenland sea or Weddell sea can have a much larger heat uptake (e.g. Banks and Gregory 2006). Offline calculations of surface flux from Fig. 3 of Banks and Gregory (2006) yield values of $O(10) \text{ Wm}^{-2}$ in these regions, consistent with projections of twenty-first century temperature change in these regions being lower than the rest of the world (e.g. Meehl et al. 2007). However, since the above regions of large oceanic heat uptake are extremely small in area since they are both longitudinally confined, and lie at high latitudes, their effects on the magnitude of φ are small.

The conceptual model can explain the results of Huntingford and Cox (2000): since even a $4\times\text{CO}_2$ perturbation has a forcing of $7\text{--}8 \text{ Wm}^{-2}$, the Q' associated with it will be less in magnitude than that associated with run 10G (see Table 1). The IGCM results suggest that a CO_2 perturbation in excess of $8\text{--}10\times$ pre-industrial values or 10 Wm^{-2} is the minimum necessary to cause large enough spatial perturbations in T'_{LFT} that significantly change φ by more than $O(0.1)$ (see Table 1). Our results are therefore consistent with φ being the same in model experiments in which CO_2 is quadrupled and doubled from pre-industrial values (Huntingford and Cox 2000).

The conceptual model shows how differences in surface properties between land and ocean act in concert with differences in land and ocean BLs to give rise to the land–sea warming contrast. When climate warms or cools, differences in evaporative fraction between land and ocean give rise to a land–sea contrast in surface energy budgets, since moisture limitations inhibit evaporation over land (Manabe et al. 1991, JGW08). However, the conceptual model suggests that such contrasts in surface energy budgets (and hence surface forcing) should be communicated to level T'_{LFT} . The spatial scale of the response in T'_{LFT} is then dependent on the spatial scale of the contrast in surface forcing: continental-scale differences in evaporative fraction between land and ocean are spread globally, but more spatially confined differences, such as those arising from physiological constraints (Joshi and Gregory 2008) give rise to more spatially confined responses.

However, lower evaporative fractions over land, as well as changes in land evaporative fraction under climate

warming, have another consequence: lapse rates over the relatively drier land change less than over ocean when climate is perturbed, directly giving rise to φ exceeding unity. In other words the effects of moisture limitation are felt locally in the BL above the surface, giving rise to a land–sea contrast in warming, i.e. $\varphi \neq 1$. This is despite the effects of the land–sea contrast in evaporative fraction under both transient and equilibrium change being communicated globally in a similar manner to the land–sea contrast in ocean heat uptake under transient climate change (Lambert and Chiang 2007).

7 Summary and conclusions

We have constructed a framework that shows that the simulated land–sea warming ratio φ in climate models changes when the imposed radiative forcing has large spatial gradients, or the globally averaged surface temperature change is much larger than that typically expected even in high greenhouse gas emission scenarios of the next century. The required spatial gradients in forcing are larger than those typically associated with global ocean heat uptake under global warming, but on a par with those typically associated with anthropogenic aerosol forcing. The framework explains the somewhat counterintuitive result that φ is projected to stay approximately invariant under transient climate change in the twenty-first century, even though historic simulations of the twentieth century show substantial changes in φ over this period (as do observations).

The conceptual model shows how the land–sea warming contrast in climate models does not arise directly from continental-scale land–ocean contrasts in surface properties such as evaporative fraction, since such effects are spread between land and ocean, but instead arises indirectly from the effects of these same land–ocean contrasts on moisture supply to the boundary layer. Future work might involve separating these direct and indirect effects in climate models to estimate the model robustness of climate response to each effect.

Finally, we note that the above results, which concern decadal timescales, could be extrapolated to shorter timescales. The presence of a seasonal cycle in extratropical land–sea temperature contrast is actually predicted by the conceptual model, because the vertical heat flux into and out of the extratropical ocean varies by over 100 Wm^{-2} annually, which significantly perturbs the diabatic heating pattern in the atmosphere, and hence changes φ compared to its value on much longer timescales. Interannual modes such as the El Niño Southern Oscillation (ENSO) are associated with much smaller changes to ocean heat uptake (Willis et al. 2004), but are strongly regionally confined in a similar manner to anthropogenic aerosol forcing, so

would also change φ . Future work might therefore consist of examining the behaviour of φ on interannual timescales vs decadal timescales in climate models, or ensembles of climate models.

Acknowledgments Manoj Joshi was supported by the UK National Centres for Atmospheric Science (Climate). Mark Webb was supported by the Joint DECC/Defra Met Office Hadley Centre Climate Programme (GA01101). We acknowledge Jonathan Gregory for very useful discussions, Yoko Tsushima for providing the HadGEM2 integration and diagnostics, and David Long and Joe Osborne for providing processed CMIP5 data. We would like to thank the reviewers of this manuscript for very useful suggestions. We acknowledge the World Climate Research Programme's Working Group on Coupled Modelling, which is responsible for CMIP, and we thank the climate modeling groups (listed in Table 2 of this paper) for producing and making available their model output. For CMIP the U.S. Department of Energy's Program for Climate Model Diagnosis and Intercomparison provides coordinating support and led development of software infrastructure in partnership with the Global Organization for Earth System Science Portals.

References

- Ackerley D, Booth BBB, Knight SHE, Highwood EJ, Frame DJ, Allen MR, Rowell DP (2011) Sensitivity of twentieth-century sahel rainfall to sulfate aerosol and CO₂ forcing. *J Clim* 24:4999–5014
- Andrews T, Forster PM, Gregory JM (2010) A surface energy perspective on climate change. *J Clim* 22:2557–2570
- Bala G, Caldeira K, Nemani R, Cao L, Ban-Weiss G, Shin H-J (2011) Albedo enhancement of marine clouds to counteract global warming: impacts on the hydrological cycle. *Clim Dyn* 37:915–931. doi:10.1007/s00382-010-0868-1
- Banks HT, Gregory JM (2006) Mechanisms of ocean heat uptake in a coupled climate model and the implications for tracer based predictions of ocean heat uptake. *Geophys Res Lett* 33:L07608. doi:10.1029/2005GL023522
- Boucher O, Lohmann O (1995) The sulfate-CCN-cloud albedo effect. *Tellus* 47:281–300
- Budyko MI (1969) The effect of solar radiation variations on the climate of the earth. *Tellus* 21:611–619
- Byrne MP and O'Gorman PA (2013) Land–ocean contrast over a wide range of climates: convective quasi-equilibrium theory and idealized simulations. *J Clim* (in press)
- Cnossen I, Lu H, Bell CJ, Gray LJ, Joshi MM (2011) Solar signal propagation: the role of gravity waves and stratospheric sudden warmings. *J Geophys Res* 116. doi:10.1029/2010JD014535
- Dommenget D, Flöter J (2011) Conceptual understanding of climate change with a globally resolved energy balance model. *Clim Dyn* 37:2143–2165. doi:10.1007/s00382-011-1026-0
- Dong B-W, Gregory JM, Sutton RT (2009) Understanding land–sea warming contrast in response to increasing greenhouse gases. Part I: transient adjustment. *J Clim* 22:3079–3097
- Doutriaux-Boucher M, Webb MJ, Gregory JM, Boucher O (2009) Carbon dioxide induced stomatal closure increases radiative forcing via a rapid reduction in low cloud. *Geophys Res Lett* 36:L02703. doi:10.1029/2008GL036273
- Drost F, Karoly D, Braganza K (2012) Communicating global climate change using simple indices: an update. *Clim Dyn* 39:989–999
- Fasullo JT (2010) Robust land–ocean contrasts in energy and water cycle feedbacks. *J Clim* 23:4677–4693
- Forster PM, De F, Blackburn M, Glover R, Shine KP (2000) An examination of climate sensitivity for idealised climate change experiments in an intermediate general circulation model. *Clim Dyn* 16:833–849
- Forster P, Ramaswamy V, Artaxo P, Bernsten T, Betts R, Fahey DW, Haywood J, Lean J, Lowe DC, Myhre G, Nganga J, Prinn R, Raga G, Schulz M, Van Dorland R (2007) Changes in atmospheric constituents and in radiative forcing. In: Solomon S, Qin D, Manning M, Chen Z, Marquis M, Averyt KB, Tignor M, Miller HL (eds) *Climate change 2007: the physical science basis. Contribution of working group I to the fourth assessment report of the intergovernmental panel on climate change*. Cambridge University Press, Cambridge, UK and New York, NY, USA
- Groisman PY, Karl TR, Knight RW (1994) Observed impact of snow cover on the heat balance and the rise of continental spring temperatures. *Science* 263:198–200. doi:10.1126/science.263.5144.198
- Holton JR (1992) *An introduction to dynamic meteorology*. Academic press, San Diego
- Huntingford C, Cox PM (2000) An analogue model to derive additional climate change scenarios from existing GCM simulations. *Clim Dyn* 16:575–586
- Hwang Y-T, Frierson DMW (2010) Increasing atmospheric poleward energy transport with global warming. *Geophys Res Lett* 37:L24807. doi:10.1029/2010GL045440
- Jones A, Haywood J, Boucher O (2009) Climate impacts of geoengineering marine stratocumulus clouds. *J Geophys Res* 114:D10106. doi:10.1029/2008JD011450
- Joshi MM, Gregory JM (2008) The dependence of the land–sea contrast in surface climate response on the nature of the forcing. *Geophys Res Lett* 35:L24802. doi:10.1029/2008GL036234
- Joshi MM, Gregory JM, Webb MJ, Sexton DMH, Johns TC (2008) Mechanisms for the land–sea warming contrast exhibited by simulations of climate change. *Clim Dyn* 30:455–465
- Kiehl J, Schneider T, Rasch P, Barth M, Wong J (2000) Radiative forcing due to sulfate aerosols from simulations with the national center for atmospheric research community climate model, version 3. *J Geophys Res* 105:1441–1457
- Lambert FH, Allen MR (2009) Are changes in global precipitation constrained by the tropospheric energy budget? *J Clim* 22:499–517
- Lambert FH, Chiang JCH (2007) Control of land–ocean temperature contrast by ocean heat uptake. *Geophys Res Lett* 34:L13704. doi:10.1029/2007GL029755
- Lambert FH, Webb MJ, Joshi MM (2011) The relationship between land–ocean surface temperature contrast and radiative forcing. *J Clim* 24:3239–3256
- Laurian A, Drijfhout SS, Hazeleger W, Van den Hurk B (2010) Response of the Western European climate to a collapse of the thermohaline circulation. *Clim Dyn* 34:689–697. doi:10.1007/s00382-008-0513-4
- Lohmann U, Feichter J (2005) Global indirect aerosol effects: a review. *Atmos Chem Phys* 5:715–737
- Lu J, Cai M (2010) Quantifying contributions to polar warming amplification in an idealized coupled general circulation model. *Clim Dyn* 34:669–687
- Manabe S, Stouffer RJ, Spelman MJ, Bryan K (1991) Transient responses of a coupled ocean-atmosphere model to gradual changes of atmospheric CO₂ part I: annual mean response. *J Clim* 4:785–818
- Martin GM, Bellouin N, Collins WJ, Culverwell ID, Halloran PR, Hardiman SC, Hinton TJ, Jones CD, McDonald RE, McLaren AJ, O'Connor FM, Roberts MJ, Rodriguez JM, Woodward S, Best MJ, Brooks ME, Brown AR, Butchart N, Dearden C, Derbyshire SH, Dharssi I, Doutriaux-Boucher M, Edwards JM, Falloon PD, Gedney N, Gray LJ, Hewitt HT, Hobson M, Huddleston MR, Hughes J, Ineson S, Ingram WJ, James PM,

- Johns TC, Johnson CE, Jones A, Jones CP, Joshi MM, Keen AB, Liddicoat S, Lock AP, Maidens AV, Manners JC, Milton SF, Rae JGL, Ridley JK, Sellar A, Senior CA, Totterdell IJ, Verhoef A, Vidale PL, Wiltshire A (2011) The HadGEM2 family of met office unified model climate configurations. *Geosci Model Dev* 4:723–757
- Meehl GA, Stocker TF, Collins WD, Friedlingstein P, Gaye AT, Gregory JM, Kitoh A, Knutti R, Murphy JM, Noda A, Raper SCP, Watterson IG, Weaver AG, Zhao Z-C (2007) Global climate projections. In: Solomon S, Qin D, Manning M, Chen Z, Marquis M, Averyt KB, Tignor M, Miller HL (eds) *Climate change 2007: the physical science basis. Contribution of working group I to the fourth assessment report of the intergovernmental panel on climate change*. Cambridge University Press, Cambridge, UK and New York, NY, USA
- Mitchell JFB, Johns TC (1997) On modification of global warming by sulfate aerosols. *J Clim* 10:245–267
- North GR (1975) Theory of energy-balance climate models. *J Atmos Sci* 32:2033–2043
- North GR, Cahalan RF, Coakley JA Jr (1981) Energy balance climate models. *Rev Geophys Space Phys* 19:91–121
- Raper SCB, Gregory JM, Stouffer RJ (2002) The role of climate sensitivity and ocean heat uptake on AOGCM transient temperature response. *J Clim* 15:124–130
- Reddy K, Pant P, Phanikumar DV, Dumka UC, Kumar YB, Singh N, Joshi H (2011) Radiative effects of elevated aerosol layer in Central Himalayas. *Int J Remote Sens* 32:9721–9734
- Rowell DP, Jones RG (2006) Causes and uncertainty of future summer drying over Europe. *Clim Dyn* 27:281–299. doi:10.1007/s00382-006-0125-9
- Shindell D, Faluvegi G (2009) Climate response to regional radiative forcing during the twentieth century. *Nat Geosci* 2:294–300
- Shindell D, Schulz M, Ming Y, Takemura T, Faluvegi G, Ramaswamy V (2010) Spatial scales of climate response to inhomogeneous radiative forcing. *J Geophys Res* 115:D19110. doi:10.1029/2010JD014108
- Sutton RT, Dong B-W, Gregory JM (2007) Land–sea warming ratio in response to climate change: IPCC AR4 model results and comparison with observations. *Geophys Res Lett* 34:L02701. doi:10.1029/2006GL028164
- Taylor KE, Stouffer RJ, Meehl GA (2012) An overview of CMIP5 and the experiment design. *Bull Am Meteor Soc* 93:485–498. doi:10.1175/BAMS-D-11-00094.1
- Weaver AJ, Eby M, Wiebe EC, Bitz CM, Duffy PB, Ewen TL, Fanning AF, Holland MM, MacFadyen A, Matthews HD, Meissner KJ, Saenko O, Schmittner A, Wang H, Yoshimori M (2001) The UVic earth system climate model: model description, climatology and application to past, present and future climates. *Atmos Ocean* 39:361–428
- Williams KD, Jones A, Roberts DL, Senior CA, Woodage MJ (2000) The response of the climate system to the indirect effects of anthropogenic aerosol. *Clim Dyn* 17:845–856
- Willis JK, Roemmich D, Cornuelle B (2004) Interannual variability in upper ocean heat content, temperature, and thermocline expansion on global scales. *J Geophys Res* 109:C12036. doi:10.1029/2003JC002260
- Yoshimori M, Broccoli AJ (2008) Equilibrium response of an atmosphere-mixed layer ocean model to different radiative forcing agents: global and zonal mean response. *J Clim* 21:4399–4423. doi:10.1175/2008JCLI2172.1